Synthesis and characterization of Si/Cs/O nanocluster thin films with negative electron affinity

L. N. Dinh, W. McLean II, M. A. Schildbach, and M. Balooch
Lawrence Livermore National Laboratory, Livermore, California 94551
(Received 21 July 1998; revised manuscript received 25 January 1999)

Patterned and unpatterned thin films of Si/Cs/O nanoclusters have been synthesized by the technique of supersaturated thermal vaporization of Si and Cs in an oxygen background gas. These films, which were deposited onto conducting or semiconducting substrates, exhibit negative electron affinity (NEA) as evidenced by ultraviolet photoemission spectroscopy. Photo, secondary, and field electron emission properties of these nanocluster films were investigated with photoelectron emission microscopy, field electron emission microscopy, secondary electron microscopy, and current-voltage measurements. Flat cathodes covered with thin films of Si/Cs/O nanoclusters exhibited high current outputs and lower turn-on fields (<8.7 V/μm) than most NEA diamond surfaces and gated Si or Mo tip arrays. The films' NEA is unaffected by air exposure and is stable to high-temperature annealing (550 °C). The electron emission property of the NEA nanocluster films can be best explained by a subband gap abundant surface-state nanocluster model. A field-emission display unit with a simple diode structure containing a flat cathode coated with a thin film of Si/Cs/O nanoclusters has also been built to demonstrate the potential application of this material in cold cathode electron emitting devices, particularly field-emission flat panel displays. [S0163-1829(99)03823-0]

I. INTRODUCTION

Theoretical and experimental studies of the phenomenon of negative electron affinity (NEA), in which the vacuum energy level lies below that of the conduction-band minimum, have been reported.[1–18] In most cases, only certain well prepared and highly oriented surfaces of some semiconductors or insulators [most notably: diamond (100) and (111), Si(001), and GaAs (100) surfaces] exhibit NEA. The preparation of these surfaces usually requires etching and high-temperature annealing in an ultrahigh vacuum (UHV) chamber. The clean surfaces are then, in the case of diamond, terminated with hydrogen or coated with well ordered layers of cesium or cesium oxide. Diamond has also been coated with metals such as Ni, Cu, Co, or Ti. In all cases, surface dipole formation is thought to induce a strong NEA. However, most of these NEA surfaces tend to be unstable when exposed to air or under prolonged electron emission. Many do not survive the thermal conditions associated with device manufacturing and packaging. Furthermore, due to the large band gaps associated with insulators, electron supply to insulating materials such as diamond for electron emission is not a trivial issue. Recently, there have been reports on NEA surfaces of AlN and $Al_xGa_{1-x}N$ epitaxially grown on α(6H)-SiC(0001) substrates.[5,6] There was no effort to control the surface termination for these samples mentioned by the authors in obtaining NEA, but lattice matching for epitaxial growth limits the number of useful substrates these NEA films can be grown on. Additionally, NEA from *e*-beam deposited BN has been reported.[4] However, there has been no report of a NEA Si-based material that is capable of producing strong electron emission, stable with respect to environment and temperature, and yet does not require a stringent surface preparation or epitaxial growth. Such a Si-based material would be an excellent candidate for applications in cold/photocathode emitters, and ready for integration into the existing silicon manufacturing technology base.

In this paper, we show how Si/Cs/O nanocluster films with NEA and stable electron emission can be easily produced by the technique of supersaturated thermal vaporization. The composition and properties of the films as a function of changing temperature and environment are evaluated. Unlike the NEA surfaces discussed above, we find that an ordered surface structure is not necessary for the Si/Cs/O nanoclusters. The NEA reported here is likely an intrinsic property of the Si/Cs/O nanoclusters. We present the electron emission properties of such Si/Cs/O nanocluster films under electron bombardment, ultraviolet photon absorption, and applied electrostatic field. A model to explain the emission property of the Si/Cs/O nanocluster material is then proposed. This paper reports on a Si-based compound nanocluster material that exhibits a stable NEA. This material has potential applications in flat panel displays and electron emitting vacuum electron devices.

II. EXPERIMENTS

The technique of supersaturated thermal vaporization has been used to produce Si nanoclusters and is described elsewhere.[19] To make Si/Cs/O nanoclusters instead of Si nanoclusters, a Cs boat was added to the system facing the Si boat. This Cs boat was coevaporated with the Si boat in a background gas of oxygen. The average size and composition of the clusters synthesized by this technique can be varied by changing the Si and/or Cs source temperatures, the oxygen buffer gas pressure, the source to substrate distance, or a combination of all these parameters. Nanoclusters generated by this technique can be deposited onto any substrate as thin films. In this report, the Si/Cs/O nanoclusters were deposited onto flat conducting or semiconducting substrates such as Si(100) wafers, the basal plane of highly oriented pyrolytic graphite (HOPG), and carbon coated Si(100) wafers. The Si(100) wafer and the basal plane of HOPG were chosen because they provide atomically flat surfaces for mi-

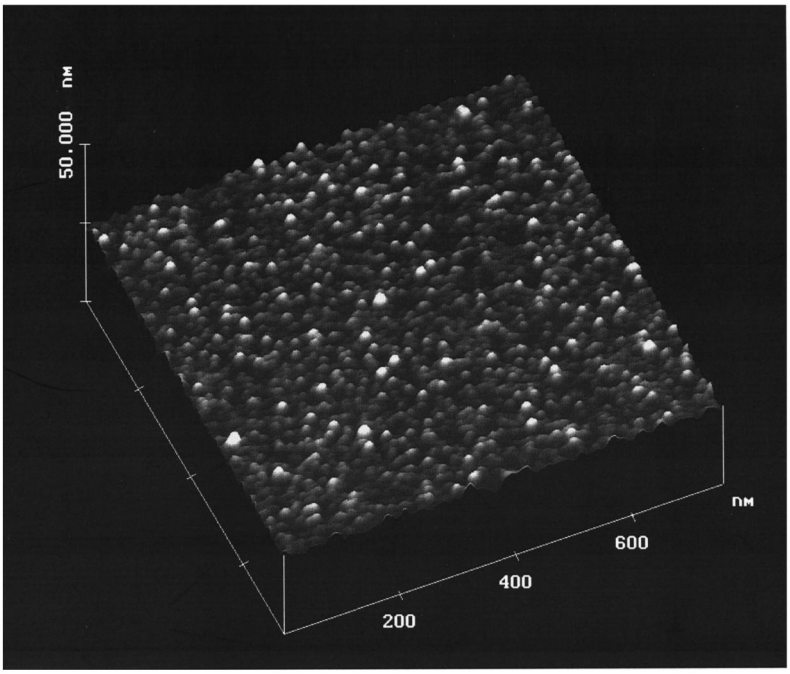

FIG. 1. AFM image of a typical Si/Cs/O nanocluster thin film. This film has a thickness of 9 nm and an average cluster size of 5 ± 2 nm.

croscopy, while thin carbon overcoats on Si(100) surfaces improve the electrical conductivity. For transmission or photoabsorption measurements, the Si/Cs/O nanoclusters were deposited directly onto a quartz substrate. The patterned films in this experiment were fabricated with the aid of a tungsten mask having regularly spaced circular holes of 125 μm diameter. The distance between the centers of any two circular holes on this mask is 250 μm.

After deposition, the samples were removed from the synthesis chamber and transported in air to the analysis chamber, which was also an UHV chamber with a base pressure of $<6.7\times10^{-8}$ Pa. This chamber was equipped with a double pass cylindrical mirror analyzer (Physical Electronics 15-255 GAR), for Auger electron spectroscopy (AES), x-ray photoelectron spectroscopy (XPS), and ultraviolet photoelectron spectroscopy (UPS). AES and XPS spectra were generated with a 3 KeV incident electron current and a Mg Kα x-ray (1253.6 eV) source, respectively. UPS spectra were produced with the He I resonance line at 21.2 eV. A photoelectron emission microscope (PEEM), PEEM 150 C from Staib Instrumente, was also attached to this UHV chamber. In the PEEM mode, a mercury lamp is employed to generate photoelectrons and secondary electrons from the surface of a grounded sample, which is positioned a few millimeters in front of the transfer case of the PEEM (at 5–15 kV above ground potential). The ejected electrons are a combination of field emitted electrons, photoelectrons and secondary electrons. They are accelerated toward the PEEM, go through a set of magnifying electrostatic lenses, and ultimately impinge onto a microchannel plate. In the field electron emission microscope (FEEM) mode, the UV lamp is not turned on so that the image formed on the microchannel plate is due solely to field-emitted electrons (under an applied electrostatic field of 1–10 V/μm) from the sample's surface. In either mode, the image formed on the microchannel plate is related to the local work function and electron affinity of the sample's surface.

The average size of the clusters that made up the films was determined by height measurement[20] with an atomic force microscope (AFM), Nanoscope III from Digital Instruments, in tapping mode. Secondary electron microscope (SEM) images and surface elemental maps of the samples were obtained using a Physical Electronics 660 scanning Auger microprobe (SAM). All post-deposition annealings were done in the analysis chamber and the temperatures were measured with an infrared optical pyrometer.

For the current-voltage characteristic curves, the end of a highly polished stainless steel cylinder with a cross section of 3 mm was employed as the anode, while the sample under investigation was negatively biased. In this exercise, the cathode to anode distance was controlled by a micrometer and measured with an optical microscope.

A demonstration flat panel display employing a diode structure was also assembled. In this structure, a Si/Cs/O nanocluster film on a carbon coated Si substrate was used as the cathode and a piece of glass coated with a thin layer of ITO (indium tin oxide) was used as the anode. Ceramic spacers of about 300 μm in thickness were sandwiched between the anode and cathode, while the edges of the cathode were covered with thin Mylar strips to prevent emission from the edges of the cathode. The diode structure was then put inside a high vacuum chamber (1.5×10^{-6} Pa). Connections to the anode and cathode were made possible by two high-voltage vacuum feedthroughs. Shunt resistors were also inserted in the wiring of the anode and the cathode to suppress arcing.

III. RESULTS

A. Physical and chemical properties

Figure 1 shows a tapping mode AFM image of an area

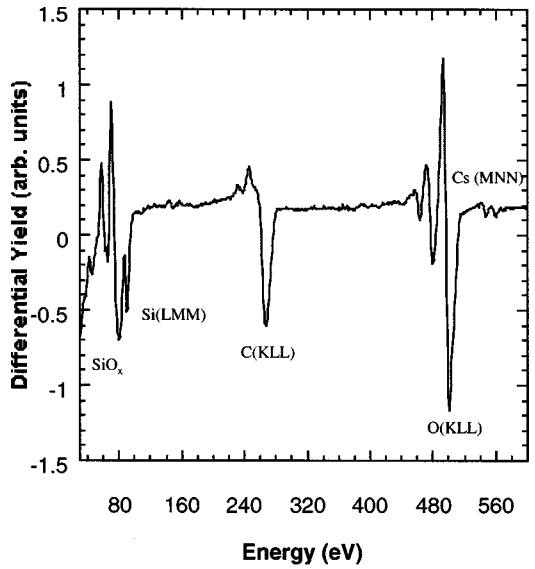

FIG. 2. AES spectrum of a 9-nm-thick Si/Cs/O film, with an average cluster size of 5 nm, on a Si(100) wafer.

typical of the surface morphology of the Si/Cs/O nanocluster thin films. This 9-nm-thick film was composed of clusters with an average size of 5 ± 2 nm.[20] The clusters were so compactly deposited that they resemble a dense array of very sharp tips.

The AES spectrum of a 9-nm-thick film, with an average cluster size of 5 nm, on a Si(100) wafer is shown in Fig. 2. The negative peak around 272 eV is the C (KLL) Auger transition which is a result of prolonged air exposure of the sample. Seven other peaks are seen in Fig. 2, at around 47, 60, 80, 92, 503, 563, and 575 eV. The peak at about 92 eV is from the Si (LMM) Auger transition, while the peaks near 60 and 80 eV are signatures of SiO_2 and SiO_x ($0<x\leqslant2$), respectively. The double peaks near 563 and 575 eV are from the Cs (MNN) Auger transition. The 47 eV peak is also a signature of cesium. The peak near 503 eV is due to O(KLL) Auger transition. The ratio (corrected for elemental sensitivity) of $Si/SiO_x/Cs/O$ from this AES spectrum is 0.80/1.00/0.15/1.11. No information on the chemical state of cesium could be inferred from AES, so XPS of cesium in these compound clusters was performed. In Fig. 3, the XPS

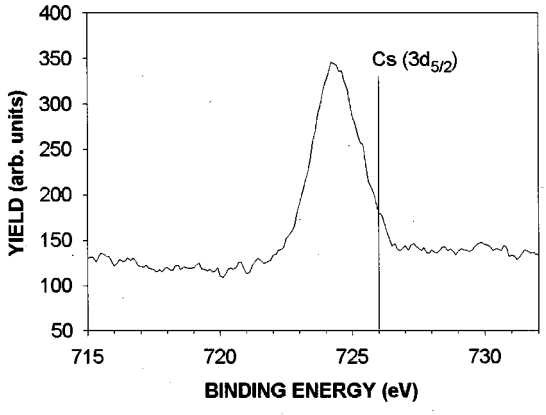

FIG. 3. Typical XPS spectrum of Cs ($3d_{5/2}$) in the Si/Cs/O compound nanocluster thin films. The vertical line at 726 eV represents the binding energy of metallic Cs ($3d_{5/2}$).

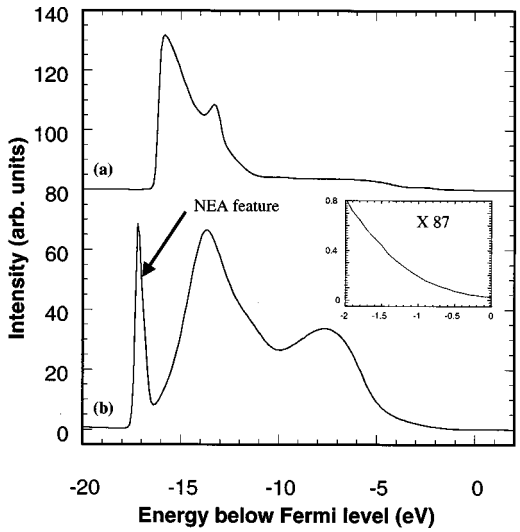

FIG. 4. UPS spectra of a clean HOPG substrate (a) and a 9-nm-thick Si/Cs/O film having an average cluster size of 5 nm on a Si(100) wafer (b). The inset shows the magnified region near the valence-band maximum of the Si/Cs/O compound nanocluster thin film.

spectrum of Cs ($3d_{5/2}$) in a typical Si/Cs/O thin film sample is shown. Note that this peak has been shifted by about 1.6 eV toward lower binding energy in comparison with metallic cesium. This behavior has been documented for cesium bonding to an oxide.[21,22]

B. UPS and NEA

Figures 4(a) and (b) show the UPS spectra of a clean HOPG substrate and a 9-nm-thick Si/Cs/O nanocluster thin film (same sample as in Figs. 2 and 3) on a Si(100) wafer. The work function of the clean HOPG substrate was determined to be 5.1 ± 0.1 eV according to the equation[23]

$$e\phi=h\nu-\Delta E. \tag{1}$$

Here, $h\nu$, $e\phi$, and ΔE are the incident photon energy, the work function, and the width of the UPS spectrum (from Fermi level to the lowest kinetic energy cutoff), respectively. The features seen in UPS spectra are related to the occupied electronic density of states of the materials under study.[23] In Fig. 4(a), the peak around 13.3 eV below the Fermi level is due to the σ conduction band of graphite. In Fig. 4(b), the broad peak around 7 eV below the Fermi level is from O($2p$). The Cs ($5p$) core level is associated with a broad peak at about 12 eV below the Fermi level and is barely seen in Fig. 4(b) due to the low Cs concentration in this sample. The peaks around 15 eV in Fig. 4(a) and around 14 eV in Fig. 4(b) are due to secondary electrons. For a material with NEA, an extra and sharp feature is expected at the lowest kinetic energy of the spectrum. This lowest energy feature is usually associated with electrons that are excited into the conduction band by photon absorption, then scatter or relax to the conduction-band minimum and subsequently fall down to the vacuum energy level (which is below the conduction-band minimum for a NEA material). We see this NEA feature in Fig. 4(b) at about 17.3 eV. When this happens, the relationship between the incoming photon energy $h\nu$, the

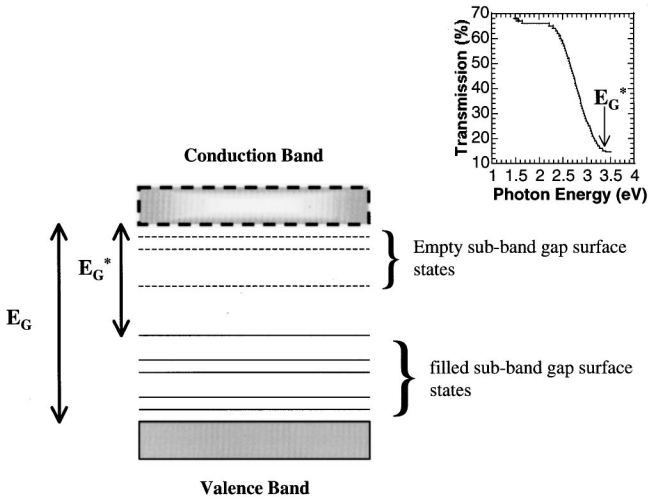

FIG. 5. Qualitative energy-band diagram of a nanocluster with abundant subband-gap surface states. The inset shows the normalized transmission spectrum of a 9-nm-thick Si/Cs/O film having an average cluster size of 5 nm on a 1.6-mm-thick quartz substrate.

energy difference between the valence-band maximum, and the lowest kinetic energy cutoff of the spectrum W, and the band-gap energy E_G can be written as[6]

$$0 = h\nu - E_G - W. \tag{2}$$

Equation (2) is, however, ill suited for NEA nanocluster materials which have abundant subband-gap surface states.[19,24–29] The inset of Fig. 4 shows the magnified UPS spectrum near the Fermi level for the 9-nm-thick Si/Cs/O nanocluster film. There, it is not possible to locate the top of the valence band, since there are filled states all the way to the Fermi level. This is physically reasonable, because, as the diameter of a cluster is reduced to the nanometer regime, the ratio of the surface atoms to bulk atoms increases significantly (this ratio is roughly about 24% for a Si nanocluster with a diameter of 5 nm). Practically, for this nanocluster film, we can say that it is the subband-gap surface states that pin down the Fermi level. So, for NEA nanocluster materials with abundant subband gap surface states, Eq. (2) can be modified to read as follows:

$$0 = h\nu - E_G^* - \Delta E, \tag{3}$$

where E_G^* is the energy difference between the pinned Fermi level and the bottom of the conduction band as illustrated in Fig. 5, while $h\nu$ and ΔE are defined as in Eq. (1). Note that subband-gap surface states do not always necessarily form discrete levels as drawn in the sketch.[19,24–29] Unfortunately, as implied in Eq. (2) and (3), the work function of a material with NEA cannot be determined by UPS according to Eq. (2) or (3).

The inset in the upper right-hand corner of Fig. 5 shows the transmission spectrum of the 9-nm-thick Si/Cs/O nanocluster film on a 1.6-mm-thick quartz substrate. The spectrum presented here has been normalized to the transmission spectrum of the same quartz substrate, which is essentially flat at about 91.5% for the photon energy range of 1–3.6 eV. The absorption onset here is seen to be very broad (from 2.4–3.4 eV) in comparison with those in bulk semiconductors such as GaAs or InSb.[30,31] Since the size distribution of the Si/Cs/O nanoclusters in this film is rather narrow (± 2 nm), the broad absorption onset here is attributed mostly to the existence of subband gap surface states as mentioned above. Photon absorption with energy less than $E_G^* = 3.4\,\text{eV}$ are thus associated with excitation of electrons within the subband-gap states, from extended valence-band states to conduction-band tail states, or from valence-band tail states to extended conduction-band states. The magnitude of the absorption strength at around $E_G^* = 3.4\,\text{eV}$ is expected to be stronger than those at lesser energies, due to a high density of empty states around the conduction-band minimum. With $E_G^* = 3.4\,\text{eV}$, $h\nu = 21.2\,\text{eV}$, and $\Delta E = 17.8\,\text{eV}$ for the 9-nm-thick Si/Cs/O nanoclusters, this sample satisfies Eq. (3) for NEA. It is important to point out that by changing the Si/Cs/O ratio and/or the average size of the constituent Si/Cs/O nanoclusters in the film, we could actually change the band gap, and thus E_G^* of the nanocluster films, and still retain the sharp NEA feature in the UPS spectra as long as the Cs concentration in the clusters is $\geqslant 5\%$.[32]

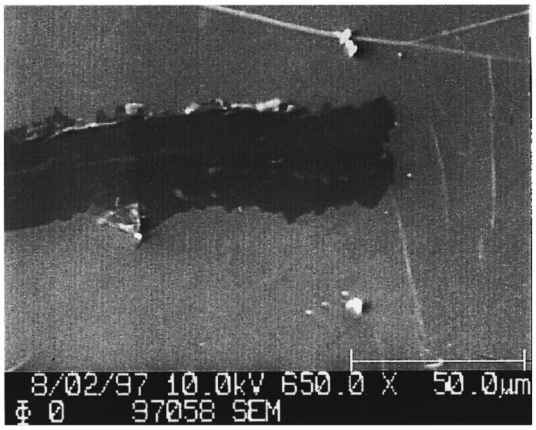

FIG. 6. SEM image of a distinct surface area of a 50-nm-thick Si/Cs/O film having an average cluster size of 5 nm on a HOPG substrate. Here, a small strip of the film has flaked off.

C. Secondary electron emission

Figure 6 shows a SEM image of a distinct surface area of a 50-nm-thick Si/Cs/O film grown on a HOPG substrate with an average constituent cluster size of 5 nm, and a $Si/SiO_x/Cs/O$ ratio of about 0.50/1.00/0.30/0.96. Here, it is observed that a small strip of the film has flaked off. SAM maps of Cs, O, Si (at 92 eV), and C taken from the same area as in Fig. 6 are shown in Figs. 7(a), (b), (c), and (d), respectively. Dark regions in SAM images represent areas that have none or very little of the elements being mapped. The black strip observed in the SEM image (Fig. 6) is then associated with a bare spot of the HOPG substrate, while the mostly bright area surrounding the strip was covered with a 50-nm-thick Si/Cs/O nanocluster film. The rather bright lines seen occasionally in the SEM image are associated with step edges from the imperfectly cleaved HOPG substrate beneath the film. The two small bright spots, one above and one below the dark strip in the SEM image, are believed to be dust particles sticking to the film due to air exposure, since these spots are void of any of the elements mapped. PEEM

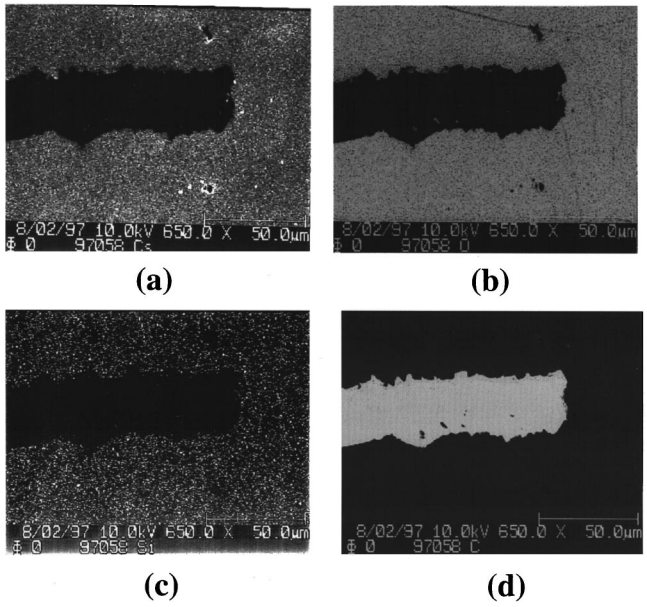

FIG. 7. SAM maps of cesium (a), oxygen (b), silicon at 92 eV (c), and carbon (d) from the same area as in Fig. 6. Dark regions in the SAM maps represent areas that have none or very little of the elements being mapped.

and FEEM (with an electrostatic field of 1 V/μm) images of a small portion of the same area seen in the SEM image of Fig. 6 are shown in Figs. 8(a) and (b), respectively. Note that, aside from some distortion,[33] the dark strip in the SEM image also appears to be dark in the PEEM and FEEM images. This implies that electrons are much more easily emitted from the Si/Cs/O nanocluster film than the HOPG substrate. This observation is consistent with the NEA indicated by the UPS spectrum of the Si/Cs/O nanocluster film.

D. Stability with respect to temperature

Figures 9 and 10 show the AES spectra and UPS spectra of a 50-nm-thick Si/Cs/O film, with an average cluster size of 5 nm, for different post-annealing temperatures. Annealing the sample for five minutes at 325 °C changed the $Si/SiO_x/Cs/O$ ratio from 0.50/1.00/0.30/0.96 [Fig. 9(a)] to 0.50/1.00/0.37/1.00 [Fig. 9(b)]. Therefore the effect of annealing at 325 °C for 5 min was a surface segregation of cesium and/or cesium oxide. Following five additional minutes of annealing at 525 °C the $Si/SiO_x/Cs/O$ ratio evolved to 0.47/1.00/0.29/1.23 [Fig. 9(c)]. This suggests a further formation of silicon oxide while some surface cesium and/or cesium oxide might have left the film surface and/or clustering up at this temperature. The C(KLL) Auger signal also increased due to intake of contaminants from the vacuum chamber upon annealing, a phenomenon we call surface carbon poisoning.[34] Note that the Cs($5p$) core level at about 12 eV below the Fermi level is more clearly seen in the UPS spectra (Fig. 10) of this Si/Cs/O nanocluster film than in the previous film, due to a higher Cs content in this sample. The secondary electron feature near the NEA peak in the UPS spectra [Figs. 10(a), (b), and (c)] of this cluster film varied in detail with annealing, but the NEA peak itself never disappeared. Therefore the Si/Cs/O compound cluster thin film exhibits a NEA that seems to be stable with annealing up to 525 °C. Furthermore, since the 50-nm-thick nanocluster film examined here is composed entirely of Si/Cs/O clusters (with a fairly uniform size distribution of 5 ± 2 nm), deposited on a highly positive electron affinity HOPG substrate, the NEA reported here is likely an intrinsic property of the Si/Cs/O clusters. However, the detailed changes of the secondary electron peak and the origin of the NEA in the cluster film are not well understood at present and require additional study.

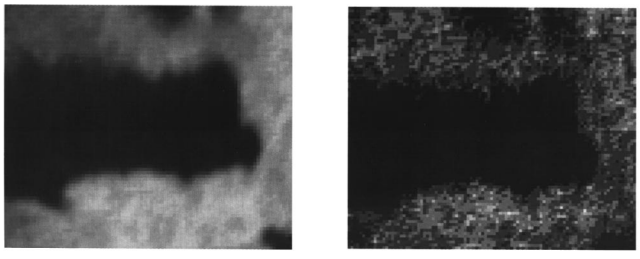

FIG. 8. PEEM (a) and FEEM (b) images of a small portion of the same area as seen in the SEM image of Fig. 6.

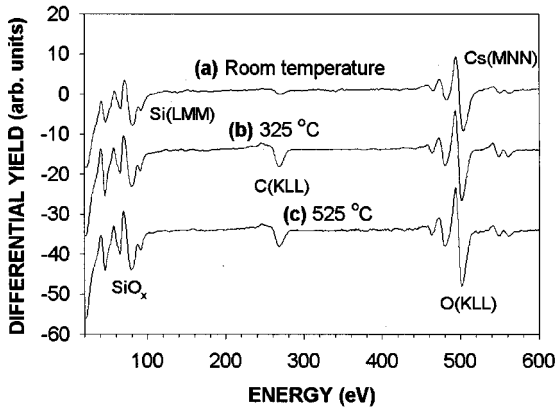

FIG. 9. AES spectra of a 50-nm-thick Si/Cs/O film, with an average cluster size of 5 nm, as a function of annealing from room temperature (a), to 325 °C for 5 min (b), and to 525 °C for 5 min (c).

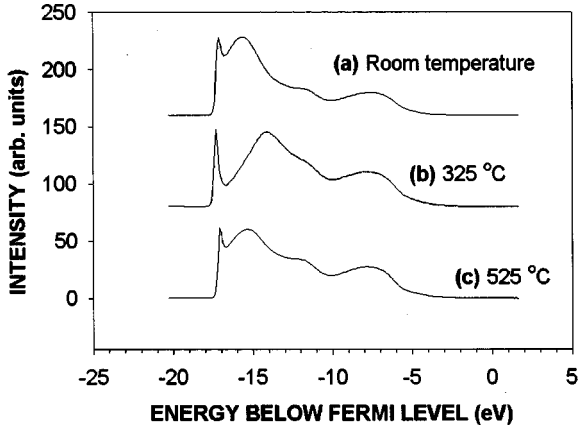

FIG. 10. UPS spectra of the Si/Cs/O nanocluster thin film in Fig. 9 as a function of annealing from room temperature (a), to 325 °C for 5 min (b), and to 525 °C for 5 min (c).

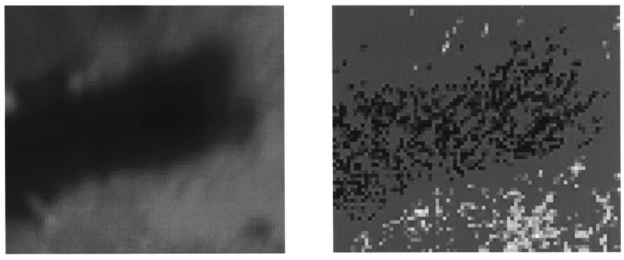

(a) PEEM (b) FEEM

FIG. 11. Room-temperature PEEM (a) and FEEM (b) images of the same area as seen in Fig. 8 after annealing to 325 °C for 5 min.

Figures 11 and 12 show the PEEM and FEEM images of the same area of the cluster film as shown in Fig. 8 after annealing. In general, the PEEM and FEEM images show clear differences in the electron emission behaviors of the bare HOPG area and the area covered with Si/Cs/O nanocluster film up to 525 °C. The area covered with the nanoclusters still readily emitted electrons after heating to 525 °C. Again, this is consistent with the NEA features observed in the UPS spectra (Fig. 10) up to this temperature. The contrast between the area covered with clusters and the bare HOPG area decreased, however, in the FEEM images with increasing annealing temperature [Figs. 8(b), 11(b), and 12(b)]. This implies a weaker field electron emission from the nanocluster film with annealing, possibly due to surface carbon poisoning and/or clustering up of cesium or cesium oxide on some surface spots. The effect of surface carbon contamination is expected to be less severe for PEEM, because the electrons detected in PEEM mode include not just surface field emitted electrons, but also photoelectrons and secondary electrons that originate within roughly 2–3 nm of the sample surface. As observed in Figs. 8(a), 11(a), and 12(a), electron emission in the PEEM mode does not show a significant degradation upon annealing. The appearance of bright spots in the PEEM image of Fig. 12 are probably a result of segregation and agglomeration of cesium (and/or cesium oxide) to the surface of the compound film upon five minutes of annealing at 525 °C. In Fig. 13, we show the SAM map of cesium in the general area of Fig. 6 after 525 °C annealing. A bright spot (high cesium content) just above the dark strip can be seen in this SAM image as well as in the PEEM image of Fig. 12. A bright rectangular area is seen in this Cs map and is corresponding to the area bombarded with an electron current of about 120 nA at 10 KeV during previous SAM imaging at a higher magnification (note the difference in the scales of Figs. 13 and 7). The high cesium level in this square area is probably due to direct electron-beam heating and/or oxygen desorption.

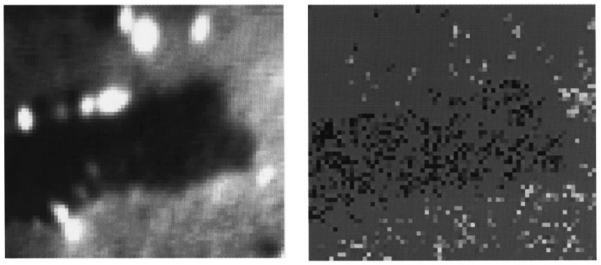

(a) PEEM (b) FEEM

FIG. 12. Room temperature PEEM (a) and FEEM (b) images of the same area as seen in Fig. 8 after annealing to 525 °C for 5 min.

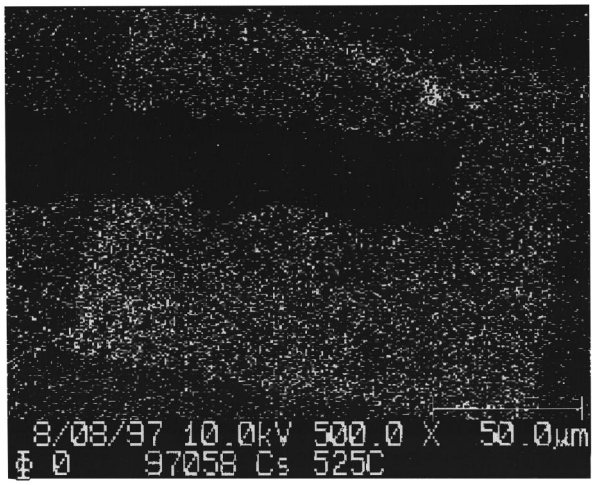

FIG. 13. SAM map of cesium from an area slightly larger than the one in Fig. 6 after annealing to 525 °C for 5 min.

E. The effect of size and composition

To see the effect of size and composition changes on the electron emission properties of the compound clusters, two Si/Cs/O nanocluster thin films were simultaneously deposited onto two 20-nm arc-deposited carbon coated Si(100). During the Si/Cs/O nanocluster deposition, one of the carbon coated Si substrates was covered by a tungsten mask as described earlier in the experiment section. The inset of Fig. 14 shows a $1750\times2500\ \mu m^2$ SEM image of the masked sample with the mask removed. Figures 14(a) and (b) represent typical AES spectra of the dark and bright areas in the SEM image. From the spectra, it is seen that the dark areas in the SEM image correspond to the carbon coated substrate, while the bright areas correspond to regions deposited with the Si/Cs/O compound material. There is very little unoxidized Si and the ratio of SiO_x/Cs/O (corrected for elemental sensitivity) in the deposited region is 1.00/0.25/1. AFM images reveal that the Si/Cs/O compound material found in this

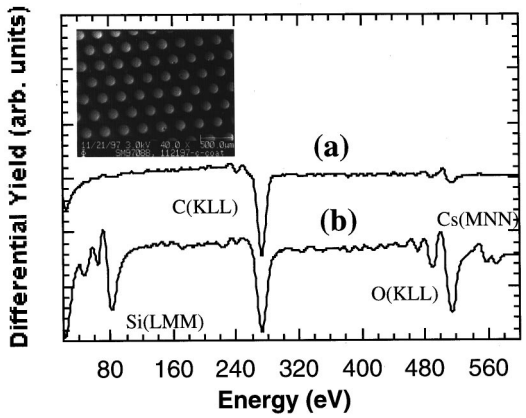

FIG. 14. AES spectra of a carbon coated Si substrate (a) and the regions deposited with 10-nm-thick Si/Cs/O film having clusters in the size range of 1–3 nm (b). The inset shows regularly spaced arrays of circular regions deposited with Si/Cs/O nanoclusters.

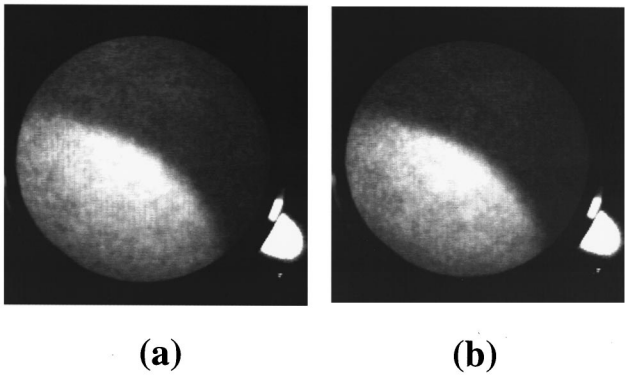

FIG. 15. PEEM (a) and FEEM (b) images of a small section of a masked sample. The regions deposited with 10-nm-thick Si/Cs/O film having clusters in the size range of 1–3 nm appear bright, while the carbon coated Si substrate appears dark in these images.

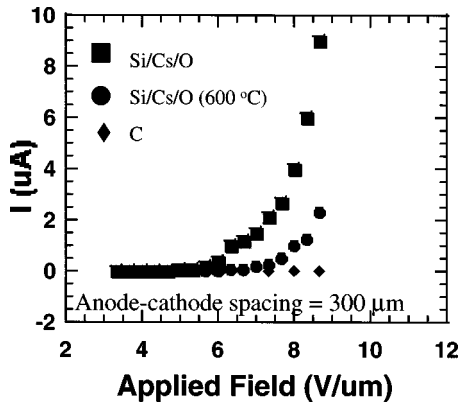

FIG. 16. Current-voltage characteristic curves for a carbon coated Si substrate (diamond dots), a 10-nm-thick unpatterned Si/Cs/O film having clusters in the size range of 1–3 nm Si/Cs/O nanocluster film on the same carbon coated Si substrate sample before (square dots) and after 600 °C heat treatment in a high-vacuum chamber (circular dots).

sample was composed of nanoclusters in the size range of 1–3 nm. UPS spectra of the unmasked sample shows features similar to those observed in the NEA Si/Cs/O nanoclusters reported earlier in this paper and will not be discussed again here. The fact that, on the masked sample, regions deposited with Si/Cs/O compound nanoclusters (about 10-nm thick) appear brighter in the SEM image implies a healthy emission of secondary electrons from the Si/Cs/O nanoclusters when bombarded with a high-voltage electron current.

Figures 15(a) and (b) show the PEEM and FEEM images, respectively, of a small section of the masked sample (the two bright spots in the lower right corner of each image were just stray room light reflected off the metal frame surrounding the PEEM's phosphor screen and accidentally recorded by the camera). In both PEEM and FEEM images, the circular regions deposited with Si/Cs/O nanoclusters appear bright while the undeposited areas appear dark. This also suggests that electron emission is much easier from the Si/Cs/O nanocluster material than from the carbon coated Si substrate. The difference in electron emission from these two regions is due to their differences in work function and electron affinity. Figure 15 also suggests that the Si/Cs/O nanocluster material has a relatively uniform emission site density. Furthermore, except for a somewhat weaker intensity, the FEEM image [Fig. 15(b)] is almost identical to the PEEM image [Fig. 15(a)]. This implies that most electrons emitted from this sample were field emitted electrons, not photo or secondary electrons. We cannot, nevertheless, exclude the possibility of photoemission in the FEEM mode due to sample absorbing scattered ultraviolet or x-ray photons generated from electrons striking the anode. It is interesting to note that the Si/Cs/O compound nanoclusters with average size of 5 ± 2 nm, reported earlier on, display substantial differences in PEEM and FEEM images (Figs. 8, 11, and 12). There, photo and secondary electrons emission are much stronger than field electron emission. The enhancement of electron field emission in the currently considered sample may be due to its smaller average cluster size of 1–3 nm (this point is presented in the discussion section on the subband-gap surface state model for NEA nanoclusters near the end of this report). However, since the Si/Cs/O ratios are also different in these two samples, such a conclusion would be premature (films prepared without Cs did not show similar behavior). More studies on the electron emission properties of this Si-based compound material as a function of cluster sizes and Si/Cs/O ratios are needed.

F. *I-V* characteristic

Current-voltage characteristic curves (Fig. 16) were obtained for a carbon coated Si substrate (diamond dots), a 10-nm-thick unpatterned Si/Cs/O film having clusters in the size range of 1–3 nm on the same carbon coated Si substrate before (square dots) and after 600 °C heat treatment in a high-vacuum chamber (circular dots). There was less than 10^{-3} μA of current drawn from the bare carbon coated Si substrate, while up to 9 μA was measured at a field of 8.7 V/μm for the Si/Cs/O nanocluster film on the same carbon coated Si substrate. The current dropped to about 2.3 μA at 8.7 V/μm after a 600 °C vacuum heat treatment. The turn-on fields obtained from the curves of Fig. 16 for our Si/Cs/O nanocluster film before and after a 600 °C vacuum heat treatment were less than 8.7 V/μm. These turn-on fields were smaller than those found for most diamond surfaces with NEA[2,3] and a factor of 5–10 smaller than Si and Mo tip arrays.[35–41] The current density drawn from our Si/Cs/O nanocluster film was also equal to or better than that from diamond surfaces with NEA.[2,3] S. P. Bozeman's group[3] has obtained $I-V$ curves for a chemical vapor deposited (CVD) diamond film, the surface of which had been terminated with hydrogen through a hydrogen plasma exposure. There, the sample area probed was 2–3 mm in diameter, and the anode-cathode distance was varied between 2.6 and 19.8 μm. The emission thresholds for these curves, defined by the authors[3] as the electric fields at which the current exceeded 0.1 μA, ranged from 28–84 V/μm, respectively.

Figure 17 shows the Fowler-Nordheim plot of the field emission $I-V$ data for our Si/Cs/O nanocluster film presented in Fig. 16. Fairly good straight line fits to the $I-V$ data points in the Fowler-Nordheim plot suggest that the $I-V$ data for the Si/Cs/O nanocluster film originated from

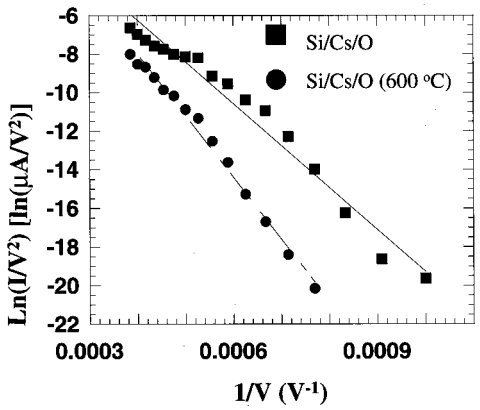

FIG. 17. The Fowler-Nordheim plot of the field-emission *I-V* data for the Si/Cs/O nanocluster film presented in Fig. 16. The symbols used here are the same as in Fig. 16. The straight lines are least-square fits to the data.

field electron emission, not space-charge effect (Child-Langmuir law). The Fowler-Nordheim relation for field emission can be written as[24]

$$\ln\left(\frac{I}{V^2}\right) = \ln(\alpha\beta) - \frac{b\phi^{3/2}}{\beta V}, \tag{4}$$

where α is related to the emission area, and to a first approximation, α and b are constants. β is the geometrical enhancement factor, and ϕ is the work function of the emitter material. From the slope and the intercept of the straight-line fits, information on the emission area, and the geometrical enhancement factor can be obtained if the work function of the material is known, and vice versa. However, the Fowler-Nordheim relationship was derived strictly for metal field emitters with positive electron affinity. Equation (4) is therefore not expected to describe field emission from NEA semiconducting or dielectric materials adequately.[42–45] Information on the dielectric constant, electron effective mass (hence energy-band structure) of the semiconducting or dielectric material is needed to properly modify the Fowler-Nordheim equation for use with nonmetallic materials.[42–47] For this reason, we are reluctant to deduce anything quantitative using Eq. (4). Currently, we are working on obtaining the structural, optical, and electronic properties of these Si/Cs/O nanoclusters using nuclear magnetic resonance (NMR), ellipsometry, x-ray absorption, and photoemission.

G. A simple diode field-emission display

In order to explore the potential use of the Si/Cs/O nanocluster material in a practical application, we have built a simple demonstration display employing a diode structure. In this display, the cathode was covered with a 10-nm-thick Si/Cs/O film with clusters in the size range of 1–3 nm. Figure 18 shows the display screen for various applied fields between the anode and cathode [0 V/μm (a), 8 V/μm (b), 9.6 V/μm (c), 11 V/μm (d), 12.3 V/μm (e)]. At an applied field of about 8 V/μm, many emission sites have lit up some portion of the screen (b). As the applied field was increased to 9.6 V/μm (c), 11 V/μm (d), 12.3 V/μm (e), additional emission sites became active. After the onset of new emission sites, it was observed that the applied field could be

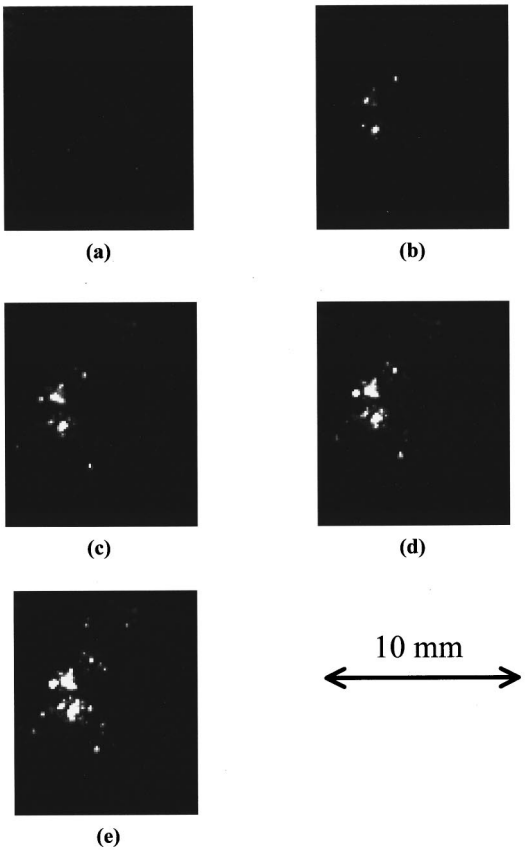

FIG. 18. The lighted display screen of a diode structure as a function of the anode-cathode applied field [0 V/μm (a), 8 V/μm (b), 9.6 V/μm (c), 11 V/μm (d), 12.3 V/μm (e)]. In this display, the cathode was covered with a 10-nm-thick Si/Cs/O film having constituent clusters in the size range of 1–3 nm.

lowered by as much as 30% without turning off any emission site. We tentatively attribute this phenomenon to desorption of water and volatile contaminants from the surface of the cathode due to air exposure. We, at times, also observed arcing where the insulating spacers coming into contact with the cathode and/or ITO screen. Such arcing was damaging to the film surface nearby, and often turned those areas off for good. Furthermore, limitations in our admittedly crude setup prevented us from going to higher fields and possibly lighting up more of the display. Here, it is interesting to note that the PEEM and FEEM images show nearly uniform emission, yet the diode display shows emission from fewer regions. This is because PEEM and FEEM images do not require high operating fields (electrons emitting from the sample are amplified and accelerated inside the microscope before striking the PEEM's phosphor screen on the back of a microchannel plate). We therefore are engaged in the construction of an improved display structure that would allow operation at higher applied fields and without the above-mentioned edge arching problem.

IV. DISCUSSION

It is interesting to note that we did not encounter any charging problem performing Auger, UPS, XPS, PEEM, and FEEM on the Si/Cs/O nanocluster films presented in this paper, considering that they are dielectrics or semiconductors

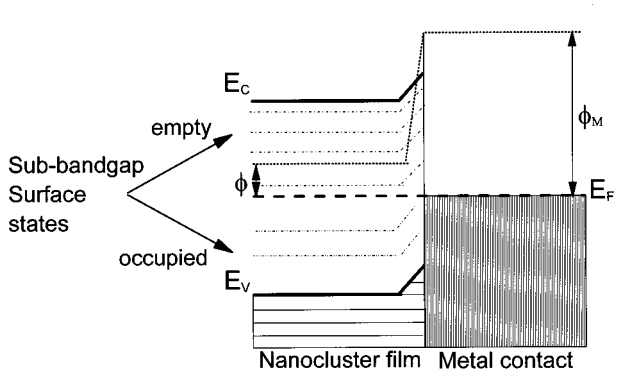

FIG. 19. Qualitative energy diagrams, including surface related traps, of a nanocluster base film with NEA grown on a metal substrate, and at thermal equilibrium. Here, ϕ, ϕ_M, E_V, E_C, and E_F stand for the work function of the nanocluster thin film, work function of the metal contact, valence-band maximum energy level of the nanocluster film, conduction-band minimum of the nanocluster film, and the Fermi level of the whole system at the equilibrium, respectively. The fine broken lines in the band-gap region of the nanocluster film represent subband-gap surface states. The band bending region near the metal/cluster film junction is due to charge transfer to align the Fermi level at equilibrium. For very thin semiconductor (or dielectric) cluster films, like the ones described in this paper, the band bending region extends throughout the film.

at best. This interesting behavior of the nanocluster films can be explained in terms of surface states with energy levels existing in the forbidden band gap. Nanoclusters have large surface-to-volume ratios, so surface states related to dangling bonds, surface stress/strain, and many other type of defects are expected to be significant. Many of these surface states, especially in the Si-based nanoclusters, are also known to have energy levels in the subband-gap region.[19,24–29] These occupied and empty subband-gap states can be most easily detected by optical techniques such as photoluminescence and photoabsorption.

The energy diagram of a NEA nanocluster thin film/metal junction is qualitatively represented in Fig. 19 (assuming NEA as an intrinsic property for these nanoclusters). In this figure, ϕ, ϕ_M, E_V, E_C, and E_F stand for the work function of the nanocluster thin film, work function of the metal contact, valence-band maximum energy level of the nanocluster film, conduction-band minimum of the nanocluster film, and the Fermi level of the whole system at thermal equilibrium, respectively. The fine broken lines in the band-gap region of the nanocluster film represent subband-gap surface states.

In the case of field emission, electrons from a metal contact or from the occupied states of the nanocluster film can come to the surface by filling up the empty subband-gap surface states. The energy barriers that these electrons have to overcome to fill up these subband-gap surface states are smaller than the energy it requires to bring the electrons to the bottom of the conduction band of the nanocluster thin film. Hence it takes a smaller field to start the field emission process from nanoclusters with abundant surface states than from larger-dimension materials. Once the field emission begins, it is through these subband-gap states that electrons from the metal contact may flow onto the cluster side (keeping the Fermi level constant across the nanocluster film/metal contact) to avoid a difficult charging problem. A similar argument can also be applied to the case of PEEM (and photocathode applications). Furthermore, if the cluster film thickness is much less than the optical penetration depth of the incoming UV photons, electrons from the metal side can absorb the incoming light as well. Many photo and secondary electrons from the metal contact can readily flow onto the nanocluster film side at the clusters/metal interface through these subband-gap surface states enhancing the emission process in the nanocluster film. Note also that as the average size of the nanoclusters is reduced, the ratio of subband-gap surface states to bulk states increases. More subband-gap surface states at the metal/NEA nanocluster film interface mean better electron flows across this junction, which translate into a more stable and enhanced field emission process. However, because of the quantum confinement effect, there are a quantization of the electronic density of states and an increase in the band gaps of nanoclusters as their sizes decrease.[19,48,49] This quantum confinement effect, consequently, negates somewhat the increase in conductivity of small nanocluster film due to subband-gap surface states.

V. CONCLUSION

We have demonstrated a technique to produce Si/Cs/O nanocluster thin films with NEA which is stable with environment and temperature up to 525 °C. However, the origin of the NEA and changes of the secondary electron peak structure in UPS spectra with annealing temperatures are not completely understood at present and require further study.

We have also presented the electron emission properties of the system of Si/Cs/O compound nanocluster films on carbon coated Si substrates. Under high-energy electron bombardment, regions deposited with Si/Cs/O compound nanoclusters on a masked sample appear brighter than the carbon substrate in the SEM image. This implies an easy emission of secondary electrons from the Si/Cs/O nanoclusters when bombarded with a high-voltage electron current. Field electron emission from the Si/Cs/O nanocluster films exhibit lower turn-on fields than most NEA diamond surfaces and Si or Mo tip arrays. The emission currents obtained from these films are equal to or greater than most NEA diamond surfaces. The cluster size/distribution and Si/Cs/O ratio seem to have an influence on the relative strength of the photo and field electron currents and requires further study. Since the presence of NEA in the Si/Cs/O nanocluster films do not require any surface termination or any ordered surface structure, the NEA here is likely an intrinsic property of the Si/Cs/O nanocluster films. Even so, the possibility of the accidental existence of some kinds of Cs related surface dipoles cannot be excluded. We report on the synthesis and electron emission properties of a Si-based nanocluster material which appears to have a great promise in electron emitting device application, particularly field-emission flat panel displays.

ACKNOWLEDGMENTS

We thank Professor F. Wooten and Dr. R. G. Musket for helpful discussions, and A. B. Balazs for some of the AFM work. This work was performed under the auspices of the U.S. Department of Energy by Lawrence Livermore National Laboratory under Contract No. W-7405-ENG-48.

[1] J. J. Uebbing and L. W. James, J. Appl. Phys. **41**, 4505 (1970).
[2] O. M. Kuttel, O. Groning, E. Schaller, L. Dietrich, P. Groning, and L. Schlapbach, Diamond Relat. Mater. **5**, 807 (1996).
[3] S. P. Bozeman, P. K. Baumann, B. L. Ward, M. J. Powers, J. J. Cuomo, R. J. Nemanich, and D. L. Dreifus, Diamond Relat. Mater. **5**, 802 (1996).
[4] M. J. Powers, M. C. Benjamin, L. M. Porter, R. J. Nemanich, R. F. Davis, J. J. Cuomo, G. L. Doll, and Stephen J. Harris, Appl. Phys. Lett. **67**, 3912 (1995).
[5] R. J. Nemanich, P. K. Bauman, M. C. Benjamin, S. W. King, J. Van der Weide, and R. F. Davis, Diamond Relat. Mater. **5**, 790 (1996).
[6] M. C. Benjamin, Cheng Wang, R. F. Davis, and R. J. Nemanich, Appl. Phys. Lett. **64**, 3288 (1994).
[7] R. L. Bell, *Negative Electron Affinity Devices* (Clarendon, Oxford, 1973).
[8] I. L. Krainsky, V. M. Asnin, and J. A. Dayton, Appl. Surf. Sci. **111**, 265 (1997).
[9] L. M. Wang, Z. Cheng, Q. Ping, and X. Hou, Appl. Phys. Lett. **67**, 91 (1995).
[10] W. E. Pickett, Phys. Rev. Lett. **73**, 1664 (1994).
[11] J. Vanderweide and R. J. Nemanich, J. Vac. Sci. Technol. B **12**, 2475 (1994).
[12] J. Sakai, G. Mizutani, and S. Ushioda, Surf. Sci. **283**, 217 (1993).
[13] T. L. Guo, J. Appl. Phys. **72**, 4384 (1992).
[14] F. Ciccacci and G. Chiala, J. Vac. Sci. Technol. A **9**, 2991 (1991).
[15] T. Abukawa, Y. Enta, T. Kashiwakura, S. Suzuki, S. Kono, and T. Sakamoto, J. Vac. Sci. Technol. A **8**, 3205 (1990).
[16] C. Bandis and B. B. Pate, Surf. Sci. **350**, 315 (1996).
[17] T. L. Guo and H. R. Gao, Appl. Phys. Lett. **58**, 1757 (1991).
[18] V. L. Alperovich, A. G. Paulish, H. E. Scheibler, and A. S. Terekhov, Appl. Phys. Lett. **66**, 2122 (1995).
[19] L. N. Dinh, L. L. Chase, M. Balooch, W. J. Siekhaus, and F. Wooten, Phys. Rev. B **54**, 5029 (1996).
[20] Due to convolution of the clusters' dimensions with the finite radius of the AFM tip, AFM diameter measurements tended to give values that are much higher than actual values. So diameter measurement is avoided here.
[21] J. F. Moulder, W. F. Stickle, P. E. Sobol, and K. D. Bomben, *Handbook of X-ray Photoelectron Spectroscopy* (Perkin-Elmer Corporation, Physical Electronics Division, Eden Prairie, Minnesota, 1992).
[22] S. Raaen, Phys. Rev. B **44**, 3373 (1991).
[23] G. Ertl and J. Kuppers, *Low Energy Electrons and Surface Chemistry* (VCH, Deerfield Beach, Florida, 1985).
[24] R. Gomer, *Field Emission and Field Ionization* (Harvard University, Cambridge, MA, 1961).
[25] Y. Kanemitsu, T. Ogawa, K. Shiraishi, and K. Takeda, Phys. Rev. B **48**, 4883 (1993).
[26] L. Tsybeskov, J. V. Vandyshev, and P. M. Fauchet, Phys. Rev. B **49**, 7821 (1994).
[27] M. Yamada, A. Takazawa, and T. Tamura, Jpn. J. Appl. Phys., Part 2 **31**, L1451 (1992).
[28] F. Koch, V. Petrova-Koch, and T. Muschik, J. Lumin. **57**, 271 (1993).
[29] G. A. Somorjai, *Principles of Surface Chemistry* (Prentice-Hall, Englewood Cliffs, NJ, 1972).
[30] C. Kittel, *Introduction to Solid State Physics*, 5th ed. (Wiley, New York, 1976).
[31] C. Weisbuch and B. Vinter, *Quantum Semiconductor Structures* (Academic, New York, 1991).
[32] L. N. Dinh, W. McLean II, M. A. Schildbach, and M. Balooch (unpublished).
[33] Under present condition in our analysis chamber, samples cannot be aligned to be satisfactorily parallel to the PEEM anode (or transfer case), hence image distortion results.
[34] M. Balooch, L. N. Dinh, and R. Musket (unpublished).
[35] G. P. Meyers, M. Aslam, P. Klimecky, L. W. Cathey, R. E. Elder, and B. E. Artz, J. Vac. Sci. Technol. B **11**, 642 (1993).
[36] D. Temple, C. A. Ball, W. D. Palmer, L. N. Yadon, D. Vellenga, J. Mancusi, and H. F. Gray, J. Vac. Sci. Technol. B **13**, 150 (1995).
[37] T. Hirano, S. Kanemaru, and J. Itoh, J. Vac. Sci. Technol. B **14**, 3357 (1996).
[38] J. M. Macaulay, I. Brodie, C. A. Spindt, and C. E. Holland, Appl. Phys. Lett. **61**, 997 (1992).
[39] F. Y. Chuang, C. Y. Sun, H. F. Cheng, C. M. Huang, and I. N. Lin, Appl. Phys. Lett. **68**, 1666 (1996).
[40] M. Q. Ding, A. F. Meyers, W. B. Choi, R. D. Vispute, S. M. Camphausen, J. Narayan, J. J. Cuomo, J. J. Hren, and J. Bruley, J. Vac. Sci. Technol. B **15**, 840 (1997).
[41] T. B. Xie, W. A. Mackie, and P. R. Davis, J. Vac. Sci. Technol. B **14**, 2090 (1996).
[42] G. Fursey, Appl. Surf. Sci. **94/95**, 44 (1996).
[43] K. L. Jensen and A. K. Ganguly, J. Appl. Phys. **73**, 4409 (1993).
[44] R. Stratton, Phys. Rev. **125**, 67 (1962).
[45] R. Schlesser, M. T. McLure, B. L. McCarson, and Z. Sitar, J. Appl. Phys. **82**, 5763 (1997).
[46] V. V. Zhirnov, G. J. Wojak, W. B. Choi, J. J. Cuomo, and J. J. Hren, J. Vac. Sci. Technol. A **15**, 1733 (1997).
[47] Y. Bu, J. C. S. Chu, and M. C. Lin, Surf. Sci. **285**, 243 (1993).
[48] T. Vanbuuren, L. N. Dinh, L. L. Chase, W. J. Siekhaus, and L. J. Terminello, Phys. Rev. Lett. **80**, 3803 (1998).
[49] For many semiconducting nanoclusters, some special surface terminations or passivations may significantly reduce the subband gap surface-states density (for example, Si nanoclusters passivated with hydrogen).